SLAC-PUB-72
February 1965

MEASUREMENT OF PION BETA DECAY BRANCHING RATIO*

Robert B. Bacastow,† Claude Ghesquière,‡ Clyde E. Wiegand
Lawrence Radiation Laboratory, University of California, Berkeley, California

and

Rudolf R. Larsen
Stanford Linear Accelerator Center, Stanford University, Stanford, California

ABSTRACT

The branching ratio for pion beta decay, $R = \frac{\pi^+ \rightarrow \pi^o + e^+ + \nu}{\pi^+ \rightarrow \mu^+ + \nu}$ was measured. Arrays of lead sheets, scintillators and spark chambers were used to measure the angular distribution of the γ rays in delayed coincidence with stopping pions. Thirty-eight events remained after subtraction of a background of 8, leading to a branching ratio of $(1.07 \pm 0.21) \times 10^{-8}$. This result is in good agreement with CVC theory and with the results of other experiments.

(Submitted to Physical Review)

*Work supported by the U. S. Atomic Energy Commission

†Present address: Physics Department, University of California at Riverside, Riverside, California

‡On leave from Ecole Polytechnique, Paris, France

A. INTRODUCTION

The Conserved Vector Current proposal of Gershstein, Zeldovich, Feynman and Gell-Mann to explain the observed near-equality of the weak coupling of the muon and the vector part of the beta decay interaction is of central importance in the description of the weak interaction. We refer the reader to the article by C. S. Wu[1] for an excellent discussion of the CVC theory and the relevant experiments.*

We simply observe that CVC predicts the branching ratio for pion beta decay

$$R = \frac{\pi^+ \to \pi^o + e^+ + \nu}{\pi^+ \to \mu^+ + \nu}, \text{ to be } R = (1.07 \pm 0.02) \times 10^{-8}.$$

This paper reports an experimental determination of R conducted at the Lawrence Radiation Laboratory 184-inch synchrocyclotron.

*This reference contains a complete bibliography of the theoretical and experimental investigations of CVC.

B. EXPERIMENTAL

1. General

Although pion beta decay, $\pi^+ \rightarrow \pi^o + e^+ + \nu$, is a very rare process, its final state contains several observable features. The detectable products of pion beta decay are the γ rays from the decay of the neutral pion and the positron. Measurable quantities include the opening angle between the two γ rays, $\theta_{2\gamma}$; the energy of the gamma rays; the energy and direction of the positrons; and the time intervals between the arrival of the pions and the occurrence of the decays. The low velocity of the neutral pions results in emission of almost collinear γ rays. Our previous experience[2] had shown that a large source of neutral pion background would be in-flight charge exchanges of positive pions. Measurement of the angle $\theta_{2\gamma}$ is a sensitive and effective method of distinguishing charge exchange π^o's from those that decay almost at rest. The present experiment relied heavily on the collinearity of the γ rays with some sacrifice of efficiency in the detection of the positrons; the experiment was not designed to measure the positron energy spectrum.

The experiment is illustrated schematically in Fig. 1. Positive pions were brought to rest in an array of scintillation counters $T_1 \ldots T_6$ sandwiched between spark chamber modules $M_1 \ldots M_7$. The spatial coordinates of the pions were indicated by the spark chambers and the times at which they stopped were shown by the counters. When a neutral pion was formed, its two γ rays were detected by an array of two sandwiches of lead sheet radiation converters, scintillation counters, and spark chambers. Pulses from all the counters were displayed on oscilloscopes.

B. EXPERIMENTAL

1. General

Although pion beta decay, $\pi^+ \rightarrow \pi^o + e^+ + \nu$, is a very rare process, its final state contains several observable features. The detectable products of pion beta decay are the γ rays from the decay of the neutral pion and the positron. Measurable quantities include the opening angle between the two γ rays, $\theta_{2\gamma}$; the energy of the gamma rays; the energy and direction of the positrons; and the time intervals between the arrival of the pions and the occurrence of the decays. The low velocity of the neutral pions results in emission of almost collinear γ rays. Our previous experience[2] had shown that a large source of neutral pion background would be in-flight charge exchanges of positive pions. Measurement of the angle $\theta_{2\gamma}$ is a sensitive and effective method of distinguishing charge exchange π^o's from those that decay almost at rest. The present experiment relied heavily on the collinearity of the γ rays with some sacrifice of efficiency in the detection of the positrons; the experiment was not designed to measure the positron energy spectrum.

The experiment is illustrated schematically in Fig. 1. Positive pions were brought to rest in an array of scintillation counters $T_1 \ldots T_6$ sandwiched between spark chamber modules $M_1 \ldots M_7$. The spatial coordinates of the pions were indicated by the spark chambers and the times at which they stopped were shown by the counters. When a neutral pion was formed, its two γ rays were detected by an array of two sandwiches of lead sheet radiation converters, scintillation counters, and spark chambers. Pulses from all the counters were displayed on oscilloscopes.

Pictures were taken of the spark chambers and oscilloscopes whenever electrically neutral radiation was detected in coincidence in the counters of both sandwiches within a time interval between 10 and 90 nsec after a pion had stopped. If a positron were also emitted by the stopped pion, it had a high probability of appearing as a pulse on the oscilloscope display of pion stopping counters. A pion beta decay was characterized by a stopping pion track and the emission of nearly collinear γ rays from the point where the pion stopped. The exact criteria by which a set of data was determined to be representative of pion beta decay are discussed in Section C.

2. Pion Counter Telescope

The detector arrangement to count the number of pions that stopped is shown in Fig. 1. It consisted of the counters S_2,$\bar{C}$,T_1 and $\bar{S}_3$ described in Table I. The Cerenkov counter responded with practically 100% efficiency to positrons. Muons in the beam had ranges in excess (~ 8 g/cm^2) of the material in the beam path and were vetoed by $\bar{S}_3$. The number of pions that stopped in the pion stopper was counted by the coincidence-anticoincidence configuration $S_2\bar{C}T_1\bar{S}_3$.

3. Pion Beam

A beryllium target of thickness 32 g/cm^2, placed in the external proton beam of the 184-inch synchrocyclotron, was the source of pions. Charged particles emitted at 25 ± 4 degrees were accepted into a magnetic spectrometer shown in Fig. 2. This system, which had a double focus at the center of the quadrupole triplet, was achromatic at the image point. Its physical length, 9 meters, corresponded to about one pion decay length

at the operating momentum of 150 MeV/c. The acceptance solid angle of the system was 6 millisteradians. The experimental value of $\Delta p/p = \pm 0.03$ was determined by transmission measurements using 100-MeV/c α particles from a radioactive source and agreed with the observed range distribution of the pions in our stopper.

The beam of positively charged particles at the stopper array had a composition of approximately 0.64 pions, 0.06 muons, and 0.30 positrons.

4. Energy Degrader

Pions entered the apparatus with a kinetic energy of 65 MeV which was dissipated in the counters of the telescope and the degrader D. Any mechanism that produced neutral pions in the vicinity of the apparatus threatened to increase the background. Positive pions can charge-exchange on the neutrons within nuclei if their kinetic energy is high enough. Ideally, liquid hydrogen should be used as the energy degrader, but this is impractical. Investigation of the properties of various nuclei revealed that carbon has a high threshold ($\approx$13 MeV) for the reaction $\pi^+ + A(Z) \rightarrow A(Z + 1) + \pi^\circ$. Therefore, CH_2 was used as the degrader; the hydrogen contributed to the stopping power but not to the background. The thickness of the degrader was adjusted to optimize the number of pion stops.

5. Gamma Ray Detectors

Gamma rays were detected by converting them to electron-positron pairs in sheets of lead. The converter sheets had to be thin enough to allow a majority of these charged particles to emerge and pass through adjacent sheets of scintillation material and, in our arrangement, spark modules. Ideally, a total of several radiation lengths of converter would be used, dispersed into thicknesses that are small in comparison with the average range of the

conversion electrons. Test measurements were made on the characteristics of tracks produced by 70-MeV γ rays as a function of lead sheet thickness. Practical limitations on the total number of sheets coupled with the results of the tests determined the choice of 0.9 g/cm^2 for the thickness of the lead sheets.

The arrangement finally adopted (Fig. 1) features twin arrays of counters, spark chambers, and converter sheets. This allows alternate sheets of scintillator to be viewed by different phototubes and permits 90° stereo viewing of the modules. The materials in each sandwich amounted to about 3.0 radiation lengths.

Scintillation counters $\bar{A}_{1,2}$ and $\bar{A}_{3,4}$ provided for the rejection of charged particles that enter the γ-ray detectors from the region of the beam. They were in electrical anticoincidence with the γ-ray counters.

6. Electronics

The primary function of the electronic logic was not to define the beta decays, but rather, was to provide a trigger for all the cameras when something that could be a beta decay occurred. For this reason reliability and efficiency were stressed rather than resolving times and speed. The components used were standard LRL type; the actual arrangement used to generate the desired trigger employed no novelties that warrant mention here.

7. Data Recording

Spark chamber pictures were recorded on a single 35-mm film within an area 24 mm × 18 mm (ciné format). The linear magnification was 0.01. Optical arrangements were conventional and consisted of plastic

field lenses adjacent to the tops and ends of the γ-ray spark chambers along with mirrors to reflect the images into the camera lens. No field lens was used on the pion-stopping spark chamber because its small size and large distance from the camera (35 ft) required no auxiliary lens. Grids ruled on transparent plastic were placed next to the lenses and were illuminated at the edges to provide a coordinate system for the spark chamber views.

Two 4-beam oscilloscopes were used to record pulses on 35-mm film from all the counters. One 4-beam tube was fed pulses from the stopping counters $T_1 \ldots T_6$ and $\bar{S}_3$. The other scope was used to record pulses from S_1, S_2, $\bar{A}_{12}$, $\bar{A}_{34}$ and the γ-ray counters. The γ-ray counter pulses that were recorded were the same as those that fed the coincidence circuits. In addition, counter S_2 was made to generate another set of pulses that were fanned out to each sweep. These pulses were the time markers to which other pulses were referred via the calibrated sweep speeds.

The sweep speed of the oscilloscope by which the stopping pion pulses were recorded was nominally 50 nsec-cm^{-1}. The other pulses were recorded by a 100-nsec-cm^{-1} sweep speed. The slower sweep speed used to record the S_1, S_2 and γ-ray pulses allowed us to inspect the output of these counters from 400 nsec before the arrival of the pion (time t_o) and for 350 nsec thereafter. (The delay time between the occurrence of an event and the breakdown of the chambers was $\approx$350 nsec.)

A set of numeral lamps was placed in each camera's field of view. All three sets were driven from the same electrical pulse and served to identify each picture.

8. Monitor Circuits

Several monitor circuits were employed to keep a continuous check on

the apparatus. One circuit monitored the number of particles through counter S_1 in the 50-nsec interval immediately preceding time t_o. The ratio of the number of these counts to the number of pions stopped depended on the cyclotron beam spill and amounted to about 0.03; that is, given a stopped pion, there was a 3% probability that an independent beam particle arrived within 50 nsec of the pion. Other circuits monitored the number of four-fold γ-ray counter coincidences and thereby provided a check on the constancy of the efficiency of the γ-ray counters. In addition, almost every run included some π^- stopping; these pictures were later studied to determine the number of observed $\pi^- + p \rightarrow \pi^o + n$ detected per stopping pion and thereby served as an over-all check on the day-to-day efficiency.

9. Tune-Up Procedure

The capture of π^- on hydrogen to yield π^o afforded a particularly nice method of preparing the apparatus to respond to beta decay events. In particular, the cable lengths (delay times) and high-voltage settings of all γ-ray counters were determined in this manner. For most of this work the π^- were stopped in CH_2, and it was soon discovered that it was necessary to do a $CH_2 - C$ subtraction; although the probability of a carbon capture yielding a detectable final state is low, the overwhelming majority of the captures are on carbon and produce an observed background of distinctly different temporal behavior. Figure 3 shows the response versus high voltage of a typical γ-ray counter.

The opening of the gate through which the γ-ray pulses passed was normally delayed by about 10 nsec to eliminate events arising from the in-flight charge-exchange of incident π^+. It was possible to trace out the gate with $\pi^- + p \rightarrow \pi^o + n$ events and to predetermine how much delay

cable was necessary to delay the opening of the gate relative to the stopping pion by any desired amount. (Results are shown in Fig. 4.)

Another method employed to eliminate triggers from in-flight generation of π^o by π^+ was to put S_1 in anticoincidence with the output of the γ counters. This was particularly effective in vetoing those instances when one π^+ stops, and another, arriving later, generates a π^o which gets through the gate opened by the previous pion. The proper delay of the S_1 signal was easily determined with $\pi^- + p \rightarrow \pi^o + n$.

It was possible to check the timings determined from $\pi^- + p \rightarrow \pi^o + n$ by removing the pion degrader and intentionally generating in-flight charge-exchange of π^+ in the stopper. The results were unchanged.

As a final check, spark chamber and oscilloscope pictures taken at several delay points of the gate were examined. We have verified that the number of acceptable π^o pictures is proportional to the number of triggers, as recorded in Fig. 4.

10. Operating Conditions

The bulk of the data was taken under the following operating conditions:

Average π^+ stopping rate	4×10^4 sec^{-1}
Duty cycle (not including the 20 Mc rf)	≈ 0.6
Ratio of pictures taken to π^+ stopped	$\approx 1.5 \times 10^{-6}$
Percentage of pictures with tracks	$\lesssim 5\%$

Most ($> 90\%$) of the triggers (pictures) could be explained as accidental coincidences between the stopping pions and uncorrelated signals from the γ-ray counters. These uncorrelated signal rates were independent of the pion beam; they originated at the accelerator and from the region of the external proton beam.

C. DATA

1. Scanning and Measuring Procedure

All spark chamber and oscilloscope film was scanned and measured in the following sequence: The spark chamber film was first viewed to find events containing tracks in the stopping chamber and both γ-ray chambers. It was required that the first pair of stopping chambers fire. A track in the γ-ray chambers was defined as any spark array containing a minimum of three sparks which included no more than two spaces between the sparks. The alignment of the sparks was further confined by requiring that the central spark be less than 2 cm (in space) from the line joining the first and third sparks and also that the projected angle between the track and the line connecting the origin of the track with the stopped pion be less than 45 degrees. This 45-degree requirement was found to have little effect on our efficiency for detecting π^{o}'s (see Section D) but was very effective in reducing the number of pictures to be measured. These criteria were applied, of course, to the direct and mirrored views of both chambers.

The oscilloscope film of those events satisfying the spark chamber requirements was then viewed to ascertain the time between the arrival of the pion and the conversion of the γ rays and also the timing of any secondary pulses in the beam counters, γ-ray counters, and anticoincidence counters. The other oscilloscope film for the same events was scanned to determine in which counter the pion stopped and the time of any possible decay pulse. It was required that any decay pulse have an amplitude of at least 1 mm on the viewer (compared to about 1/2 mm for the background). Those events which satisfied the chamber criteria, and which had no beam

particle arriving within ±10 nsec of the pulse in the γ-ray counters and for which the pulses in the stopping counters were consistent with the pattern in the stopping chamber, were measured on a Vanguard measuring projector. For each event we digitized the 10 fiducial marks, the origin of the two γ-ray tracks in both views, and the end of the stopping beam track. Simultaneously, timing information and a few yes/no comments were digitized.

Some of the scanning criteria impose efficiencies on the data which are discussed in Section D.

2. Measurement of Events

The measurements with the digitizing projector had an accuracy of about 3μ on film and introduced uncertainties which were negligible compared to other sources of error. The digitized events were processed with a reconstruction program on an IBM 7044 computer that calculated the angle between the two γ rays and the estimated error of that angle. The accuracy of the angular measurement was a linear function of the uncertainty in position of the conversion of the γ ray. Two pictures were taken at 90 degrees; therefore, the errors are identical in both projections and need be evaluated on only one projection. The grids under the field lenses provided a good map of the distortion and non-linear aberrations of the whole optical system, thus obviating the necessity of fabricating and aligning a precise optical system. Corrections were introduced into the reconstruction program to take the observed distortions into account.

Other uncertainties in coordinates not revealed by a study of the grid images were:

a. Multiple scattering: The γ-ray conversion electrons multiple-scatter in the lead sheets, resulting in an apparent displacement of the point of conversion as observed in the nearest spark module. The observed mean projected scattering angle is 15 degrees; folding in the geometry of the sandwich and the distribution of conversion points results in an estimated uncertainty of $\sigma_{scat} = 29\mu$ on the film.

b. Spark image size: The images of the sparks were about 50μ wide on film and some were irregular in shape. The uncertainty in locating the spark coordinates is estimated to be $\sigma_p = 25\mu$. This estimate was verified by making multiple measurements of a single spark and observing the resultant coordinate distribution. This uncertainty includes the inaccuracy in the measurement of the fiducial marks.

c. Apparent displacement of sparks: Sparks were observed through one-inch-thick Lucite frames on the spark modules. Although the windows were accurately machined and polished, there were some imperfections that caused apparent displacements. The error introduced was estimated by studying the dispersion of sparks along the lines of flight of cosmic rays. This error is estimated as $\sigma_d = 20\mu$ on the film.

The total estimated uncertainty in the coordinates of γ-ray conversion points is $\sigma_t = (\Sigma\sigma^2)^{\frac{1}{2}} = 43\mu$ on the film, which corresponds to ± 4.3 mm in space.

In the stopping chamber the main uncertainty is due to the stopping counter thickness, which is $\pm 25\mu$ on the film.

The errors in the coordinates of the γ-ray conversion points and the error in the coordinates of the point of origin of the γ rays cannot be combined as if they were independent because the point of origin is common to the two rays. The size of the error in the angle between the rays also depends upon the distances between the point of origin and the conversion points and upon the angle itself. If the conversions occurred deep within the spark chambers, the angle could be determined to ± 0.5 degrees; however, most conversions took place in the first few lead sheets where the angle could not always be determined to better than ± 3 degrees. A detailed study of these effects forces us to assign an average uncertainty of ± 2 degrees to $\theta_{2\gamma}$. These estimates have been checked in two ways:

a. Cosmic ray muons were used to imitate tracks that had $\theta_{2\gamma} = 180^{\circ}$. Measurements of the angle between these tracks resulted in a distribution of $\theta_{2\gamma}$ centered on 180° and characterized by a spread of ± 1.4 degrees; this observed dispersion was in agreement with our calculated uncertainty in $\theta_{2\gamma}$.

b. The distribution of the opening angle between the two γ rays, $\theta_{2\gamma}$, from the reaction $\pi^- + p \rightarrow \pi^0 + n$ was measured. About 250 events were measured and the histogram of $\theta_{2\gamma}$ (Fig. 5) was fitted to a theoretical distribution

$$N_{(\theta_1 < \theta_{2\gamma} < \theta_2)} = N \int_{\theta'=\theta_1}^{\theta'=\theta_2} d\theta' \int_{\theta=\pi}^{\theta=\theta_{2\gamma max}} \frac{(1 + \cos\theta)^{\frac{1}{2}}}{\beta\gamma(1 - \cos\theta)[\gamma^2(1 - \cos\theta) - 2]^{\frac{1}{2}}} \cdot [1 - 0.14(\pi - \theta)] \frac{1}{\sqrt{2\pi}\,\sigma_g} e^{-\frac{(\theta-\theta')^2}{2\sigma_g^2}} d\theta$$

in which the first factor is the phase space distribution, the factor $[1 - 0.14(\pi - \theta)]$ takes account of the loss in efficiency when $\theta_{2\gamma}$ decreases, and the last factor is the experimental dispersion. Parameters of the fit are σ_g and $\theta_{2\gamma max}$, where $\theta_{2\gamma max}$ is determined by the momentum of the neutral pions. The fit of the data to the theoretical distribution is rather insensitive to σ_g but strongly depends on $\theta_{2\gamma max}$. Our best fit gives $\theta_{2\gamma max} = 155.5$ degrees and $\sigma_g = 2$ degrees. From the fit we cannot conclude anything significant about σ_g, but the value of $\theta_{2\gamma max}$ is 0.6 degrees lower than the value calculated from the value of the $\pi^- - \pi^o$ mass difference.[3] We do not know if this represents a systematic error in the measurement of angles near $\theta_{2\gamma} = 155$ degrees and/or an unknown background. Because we are unable to assign this slight discrepancy to its proper place in this analysis, we simply note the discrepancy and retain ±2 degrees as the uncertainty in the angular measurements.

Having determined the accuracy of the angular measurements and knowing that $\theta_{2\gamma} \geq 176$ degrees for pion beta decay, we calculate that $\theta_{2\gamma} = 172$ degrees ($\cos \theta_{2\gamma} = -0.99$) is the maximum angle that will include essentially all the events; accordingly, we require $-1.0 \leq \cos \theta_{2\gamma} \leq -0.99$ for an acceptable event.

Pictures of the oscilloscope pulses, showing relative times of occurrence of the pions stopping and the emission of positrons and γ rays, were measured directly on the scanning table. The timing signals generated by counter S_2 were used as reference markers on all scope sweeps. The positions of the four γ-ray counter pulses that corresponded to prompt events (coincident with pion stopping) were deduced from a study of $\pi^- + p \rightarrow \pi^o + n$. In terms of the velocity of light, the size of the counters was 4 nsec × 4 nsec.

The measured average spread in γ-ray arrival time t_γ amounted to ± 2.5 nsec and includes the inaccuracy due to the width of the sweep trace. In the stopping counter the small amplitude of the decay pulse accounts for the main error; here an accuracy of ± 2.5 nsec appears conservative. Therefore, if a decay pulse were visible it was required that its time satisfy

$$\left| t_\gamma - t_{decay} \right| \leq 5 \text{ nsec}$$

in order to qualify as a beta decay event.

3. Results

In the experiment, a pion beta decay was required to display the following basic signature: a positive pion stopped in the stopping apparatus at a time $t = 0$, and in a later time interval $12 < t_\gamma < 91$ nsec (within which the gate is 100% efficient) two γ rays appeared with an opening angle $\theta_{2\gamma} \geq 172$ degrees. About 60% of these events were accompanied by a pulse in $T_1 \ldots T_6$ that came at a time t_d within ± 5 nsec of t_γ, and these pulses are ascribed to decay positrons.

There are two categories of events that fulfill the basic criteria:

a. Events with a visible decay (positron) in the stopping counter. In order to estimate the background contribution to these beta decay events, we made a scatter diagram of all events in a $(\cos \theta_{2\gamma}, t_d - t_\gamma)$ coordinate system (Fig. 6). The diagram was not extended beyond $\cos\theta_{2\gamma} = -0.65$ because the detection efficiency drops too quickly beyond that value. Beta decay events are contained in Zone III of Fig. 6. The problem is to estimate the number of background events among the 28 events in Zone III by reasonable extrapolation of the event densities in Zones I, II, and IV into Zone III. The probability of observing a given density (number

of events per $\Delta \cos \theta_{2\gamma} \equiv 0.01$) in Zone I is apparently constant in $\cos \theta_{2\gamma}$. This constant density appears to prevail in Zone II; a least squares straight line fit to the 28 events in Zone II yields 0.83 events-interval^{-1} at $\cos \theta_{2\gamma} = -1$ and a slope of 0.002 events-interval^{-2}. Figure 6 displays $\approx 90\%$ of the background. When the observed density is scaled to correspond to the total background, we find the background in Zone III to be 1.0 ± 1 event. A study of the background in the vicinity of Zone III reveals that this result is independent of the direction of the extrapolation. We conclude that there are 27 ± 1 beta decays in Zone III. The time distribution of the events in Zone III was characterized by a mean life of 25.5 ± 4 nsec.

b. In the second category of events are included all events except those that have a decay pulse satisfying $|t_d - t_\gamma| > 5$ nsec. All events which have $12 < t_\gamma < 91$ nsec are located in a $(\cos \theta_{2\gamma}, t_\gamma)$ coordinate system (see Fig. 7). The extrapolation of the best fitted straight line (corrected for the background not displayed in Fig. 7) into Zone II yields 8 background events; there are 38 ± 2 net events that we claim are beta decays.

The projection of Zone II onto the t_γ axis, as shown in Fig. 7, closely resembles the spectrum expected from pion decays. The mean life is 26.5 ± 4 nsec. More significant, however, is the observation that the spectrum is not at all consistent with the muon lifetime (or any other uniform distribution) or the 54-nsec period of the synchrocyclotron rf.

The bulk of our quantitative results are based on statistical arguments, and we cannot exclude with certainty the possibility that some other process produces the peaking in the distributions around $\theta_{2\gamma} = 180^\circ$. For this reason we consider the following reactions, which are the most likely background candidates for the observed peaking.

a. $\pi^+ \rightarrow e^+ + \nu + \gamma$. This mode has been studied theoretically by several authors[4,5] and recently some experimental results[6] have become available. Combining these results with the probability that a high-energy positron annihilates while leaving the stopper and applying our angular criterion, we calculate that less than 2% of our events are due to this decay.

b. $\pi^+ \rightarrow \mu^+ + \nu \rightarrow e^+ + \gamma + \nu$. If the π - μ decay is very rapid, the muon pulse could be concealed by the stopping pion pulse; if the muon then decayed as indicated within the gate and the positron annihilated in flight, this event would be indistinguishable from beta decay. Using 2×10^{-8} as an upper limit for the $\mu^+ \rightarrow e^+ + \gamma$ branching ratio,[7] and multiplying by the annihilation probability and the chance of decay within our gate, we calculate that less than 1% of our events could be due to this process. We also note that the time dependence of our data is inconsistent with the muon lifetime.

c. $\underline{\pi^+ \rightarrow \mu^+ + \nu \rightarrow e^+ + \nu + \bar{\nu} + \gamma + \nu}$. Radiative muon decay exhibits[8] an almost uniform spectrum in $\cos \theta_{e\gamma}$ for $\cos \theta_{e\gamma} < -0.85$. Although our efficiency for detecting low energy ($\geq$ 15 MeV) γ rays is unknown, it is possible that a large percentage of our background (Figs. 6, 7) is due to this process. We believe that our background subtraction method takes adequate account of this effect.

D. EFFICIENCY

The net efficiency for detecting a pion beta decay consists of several independent factors.

1. π^o Efficiency

The efficiency for detecting the π^o was measured with a hydrogen gas target (Fig. 8) containing counters $\bar{S}_c$ and S_L (see Table I) designed so that the number of π^- stopping in H_2 could be accurately determined. Then from published values[9] of the Panofsky ratio $(\frac{\pi^- + p \rightarrow \pi^o + n}{\pi^- + p \rightarrow \gamma + n})$, the number of π^o's produced was known. The efficiency was the ratio of detected π^o's to produced π^o's. The experimental results are contained in Fig. 9. The average value of the ratio of acceptable π^o events to pictures (triggers) was 0.60 ± 0.01. However, the criterion that the spark track from the γ-ray conversion makes an angle of less than 45 degrees with respect to the γ-ray direction in the projected images could not be applied because the precise location of the pion stop was unknown. The effect of this criterion was measured independently using π^o's from π^- stopping in the array of chambers and counters of Fig. 1 and was found to be 0.91 ± 0.03 . The probability that a trigger represents an

event satisfying the scanning criteria is then

$$F = (0.60 \pm 0.01)(0.91 \pm 0.03) = 0.55 \pm 0.02.$$

A correction factor must be applied to the π^o efficiency to account for the difference in angular correlation between the two γ rays from $\pi^- + p$ and those from pion beta decay. The γ rays from $\pi^- + p$ have a smaller average angle between them, and this lowers the probability that they will trigger the apparatus. By the Monte Carlo technique, the total conversion probability for the π^o from $\pi^- + p$ and also for the π^o from beta decay were calculated. The ratio of these two probabilities is the correction factor to be applied. The calculation began by choosing stopping coordinates for the pion; a uniform distribution for π^- stopping in H_2 was assumed, and the measured distribution for the π^+ stopping in the counter array of Fig. 1 was used. Angles for one of the photons were chosen and a calculation made of the path length of this line through one of the γ-ray spark chamber arrays. A conversion distance inside the array was chosen according to an exponential distribution, and the difference D_1 between the line length inside the chamber and the conversion distance was found. The angles of the other γ ray were chosen according to the theoretical distribution in $\theta_{2\gamma}$, and a distance D_2, similar to D_1, was calculated. The event was accepted only if D_1 and D_2 were both greater than a value D_o. The ratio of acceptable beta decay events to acceptable $\pi^- + p$ events was found to be quite independent of D_o for D_o between 7.5 cm and 12.5 cm. Because adjacent spark chamber modules were separated by about 2.5 cm and 3 sparks were required for a good event, 7.5 cm to 12.5 cm is roughly the range of interest.

All the parameters were varied. The calculation was sensitive only to the distribution in $\theta_{2\gamma}$. The conclusion of the calculation is that the measured efficiency for detecting the π^o from $\pi^- + p$ should be multiplied by 1.15 ± 0.02.

The γ rays from $\pi^- + p$ have a uniform energy spectrum extending from 55 MeV to 83 MeV; those from pion beta decay have limits of 65.3 MeV and 69.8 MeV. This difference could produce a difference in the distribution of sparks in tracks and thereby effect the efficiency. The $\pi^- + p$ events displayed in Fig. 5 were divided into two angular intervals which resulted in one group consisting of events with γ rays of nearly equal energy and another group of events with γ rays near the extremes of the allowed energy spectrum. No difference in the distribution of sparks was detected between the two groups. A study of the spark distribution of the events we claim are beta decays revealed no deviation form the distribution for the $\pi^- + p$ events. Although the samples that were studied were biased because of the scanning criteria, the tracks with a large (≥ 4) number of sparks would have revealed any significant energy dependence.

Another correction factor of 0.99 has to be applied to account for the difference in wall thickness of the hydrogen target and the stopping spark chamber. We use 0.605 ± 0.003[9] as the probability of producing a π^o when a π^- stops in hydrogen. Finally, the ratio of the slope of the number of triggers per monitor vs pressure (Fig. 9-b) to the slope of the number of π stops per monitor vs pressure (Fig. 9-a) is 0.0793 ± 0.030. All these factors were combined into an efficiency for detecting the π^o from pion beta decay

$$\pi^o \text{ efficiency} = (0.0793)(1.15)(0.55)(0.99)/(0.605) = 0.082 \pm 0.005$$

2. Efficiency Due to Gate Time

An electronic gate was opened each time a pion stopped. The gate delay was set so that the gate was half open 8 nsec after the pion stopped and fully open 12 nsec after the pion stopped. The fraction of decays between 12 and 91 nsec was $e^{-\frac{12}{25.5}} - e^{-\frac{91}{25.5}} = 0.596$. An uncertainty of 2.5 nsec in the measured time of the γ ray introduces a negligible correction in this timing efficiency.

3. Positron Efficiency

To obtain the efficiency to detect the decay positrons, measurements were made with a radioactive source of Ga^{66}, which decays mainly by positron emission with a half-life of 9.5 hours and whose energy spectrum closely approximates the spectrum of pion beta decay (maximum energy 4 Mev). It was conveniently prepared by irradiating a zinc foil 2.5 cm in diameter by 0.0025 cm thickness with protons. The total number of positrons emitted per second was counted in a 4π steradian scintillation counter. Approximately ten hours after irradiation the short-lived activities had disappeared, and the source began to decay with a 9.5-hour half-life. The foil was then placed at various positions within the stopping counter array. A counting circuit was connected to the counter leads that ordinarily went to the oscilloscope, and the threshold of the circuit was adjusted to correspond to the viewing threshold of 1 mm. The efficiency for counting a positron in the array was then calculated by averaging the measured efficiencies for the various source positions weighted by the stopping pion density at those positions. The resulting average efficiency was 0.83 ± 0.04. The uncertainty in this number is due to

the uncertainty in the stopping distribution; fortunately, the calculation is relatively insensitive to this parameter.

To obtain another estimate of the efficiency a Monte Carlo calculation was performed. The program imitated the counter geometry and pion-stopping distribution quite accurately, and generated an allowed beta spectrum of positron energies. Positron ranges were calculated by Feather's Rule:

$$R(g/cm^2) = 0.542\ T - 0.133$$

where T is the kinetic energy in MeV. The maximum energy given by the positron to one of the six counters was calculated assuming the positron follows a straight path of length corresponding to its range. If this energy were greater than 0.4 MeV (which corresponded to approximately a 1-mm deflection of the trace on the film viewer), it was assumed that the positron would be recognized. However, the straight line distance a positron goes is ordinarily much less than expected from Feather's Rule, principally because the positron multiple-scatters. The calculation was repeated with ranges of 1.0, 0.75, and 0.50 of the value given by Feather's Rule, and the resulting efficiencies were 0.85 ± 0.03, 0.82 ± 0.04, and 0.77 ± 0.04. The indicated errors are for ± 0.1 MeV in required deposited energy.

These two independent methods of determining the positron efficiency agree quite well, so we will take the positron efficiency to be 0.82 ± 0.04.

4. Miscellaneous Losses

Several other factors must be included in the efficiency. These factors are grouped together here because they represent small losses of events.

a. Events could have been vetoed by the conversion of the decay positron annihilation radiation in one of the guard counters $\bar{A}_{1,2}$ or $\bar{A}_{3,4}$. The magnitude of this effect was measured by placing the Ga^{66} source between T_3 and T_4 and noting the counting rate in $\bar{A}_{1,2}$ and $\bar{A}_{3,4}$. A simple calculation employing γ-ray attenuation lengths confirmed the resulting efficiency factor of 0.90 ± 0.02.

b. Some pions stopped outside the fiducial region of the T-chambers. The fiducial region was chosen so that pions which hit the chamber frames would be excluded from consideration. Pions which stopped beyond counter 6 were also excluded. The resulting loss in efficiency was measured by analyzing pictures of stopping pions. The pictures were taken whenever a pion stopped in accidental coincidence with a random signal generator. This was done to avoid triggering on γ rays which might have been preferentially produced when pions stopped outside the fiducial region. The efficiency factor was 0.94 ± 0.03.

c. Occasionally a second beam particle would enter the stopping chamber within the chamber resolving time and vitiate the track of the particle that produced the trigger. We were then unable to reconstruct the event, and it was rejected. The probability of this occurrence was measured by analyzing pictures of random stopping pions at the same beam level as that which prevailed during the data taking. It was found that 0.96 ± 0.01 of these events could be reconstructed, in that a track was seen to stop in the region indicated by the T counters.

d. The use of S_1 to veto prompt events results in losses when a second beam particle enters the array and vetoes a possible event. This factor is estimated to be 0.99 ± 0.01.

e. The scanning efficiency varied among the four scanners who at different times worked on the experiment; an average calculated by weighting the individual efficiencies with the percentage of film scanned by each person results in a scanning efficiency of 0.95 ± 0.01.

f. Gamma-ray conversions which were visible but outside the chamber fiducial region introduce a factor of 0.99, which is estimated from π^o's made by stopping π^-'s in the T counters.

Many effects were studied and found to contribute negligibly to the efficiency. Among these are $\bar{A}_{1,2}$ and $\bar{A}_{3,4}$ random pulses, and muons which stop within the T counters and duplicate a pion stop.

The product of all these independent factors is 0.037 ± 0.003, and this is our efficiency for detecting a pion beta decay when a visible positron is not required. If, in addition, a visible positron is required as a check on the data, the efficiency becomes 0.030 ± 0.003.

E. RESULTS

1. Branching Ratio

We first note that relinquishing the requirement of detecting the positron does not alter the branching ratio; that is, the ratio of all events to events with a positron is 1.41 ± 0.40, while the ratio of the corresponding efficiencies is 1.22 ± 0.13. This serves as an internal check on our evaluation of the efficiencies and of the background subtractions.

The 38 ± 7 detected events were produced by 9.558×10^{10} stopped pions (as read on scaler) and were detected with an efficiency of

0.037 ± 0.003. The branching ratio is then

$$R = \frac{\pi^+ \to \pi^0 + e^+ + \nu}{\pi^+ \to \mu^+ + \nu} = \frac{38 \pm 7}{(0.0370 \pm 0.0027)(9.558 \times 10^{10})} = (1.07 \pm 0.21) \times 10^{-8}$$

2. Comparison With Other Experiments

Since 1962, several laboratories have measured the pion beta decay rate. Different features of the final state have been emphasized by the various experiments. Table II lists these measurements, the number of events, the experimental emphasis, and the branching ratios. We use the prerogative of the latecomer to form a weighted average of these results, obtaining

$$R = (1.12 \pm 0.08) \times 10^{-8} .$$

ACKNOWLEDGEMENTS

We are pleased to acknowledge the continuous encouragement received from Professor Emilio Segre. Dr. William Johnson and Dr. Tom Elioff gave valuable assistance in the early stages of the experiment. Miss Doris Heyneman was very helpful and the scanners under the direction of Mrs. Louise Shreve did an admirable job.

The crew of the 184-inch synchrocyclotron, under the direction of Mr. James Vale, maintained a smoothly operating accelerator over many months of running.

LIST OF REFERENCES

1. C. S. Wu, Rev. Mod. Phys. 36, 618 (1964).
2. R. Bacastow, T. Elioff, R. R. Larsen, C. Wiegand and T. Ypsilantis, Proc. 1962 International Conference on High Energy Physics at CERN. R. Bacastow, T. Elioff, R. R. Larsen, C. Wiegand and T. Ypsilantis, Phys. Rev. Letters 9, 400 (1962).
3. A. H. Rosenfeld, A. Barbaro-Galtieri, W. H. Barkas, P. L. Bastien, J. Kirz and M. Roos, Rev. Mod. Phys. 36, 977 (1964).
4. S. A. Bludman and J. A. Young, Phys. Rev. 118, 602 (1960).
5. D. E. Neville, Phys. Rev. 124, 2037 (1961).
6. P. Depommier, J. Heintze, C. Rubbia and V. Soergel, Phys. Letters 7, 285 (1963).
7. S. Parker, H. L. Anderson and C. Rey, Phys. Rev. 133, 768 (1964).
8. C. Rey, Phys. Rev. 135, 1215 (1964).
9. James W. Ryan, Phys. Rev. 130, 1554 (1963).
10. P. Depommier, J. Heintze, A. Mukhin, C. Rubbia, V. Soergel and K. Winter, Proc. 1962 International Conference on High Energy Physics at CERN; P. Depommier, J. Heintze, A. Mukhin, C. Rubbia, V. Soergel and K. Winter, Phys. Letters 2, 23 (1962); P. Depommier, J. Heintze, C. Rubbia, V. Soergel, Phys. Letters 5, 61 (1963).
11. P. Depommier, J. Duclos, J. Heintze, K. Kleinknecht, H. Rieseberg and V. Soergel, Proc. 1964 International Conference on High Energy Physics (Dubna, USSR, 1964).
12. A. F. Dunaitsev, V. I. Petrukhin, Yu. D. Prokoshkin, V. I. Rykalia, Preprint 1559, Joint Institute for Nuclear Research, Dubna, USSR (1964).
13. D. Bartlett, S. Devons, S. L. Meyer and J. L. Rosen, Phys. Rev. 136, B1452 (1964).

TABLE I

Dimensions and Characteristics of Detector Components

Component	Function	Width (cm)	×	Height (cm)	×	Thickness (cm)
S_1	Scintillation counter	21.5	×	21.5	×	1.0
S_2	Scintillation counter			11.4 diam	×	1.6
$\bar{C}$	Cerenkov counter ($\beta_{min} \approx 0.8$)	12.7	×	12.7	×	3.5
D	Energy degrader CH_2	10.1	×	10.1	×	6.0
T_1	Scintillation counter			7.6 diam	×	0.5
$T_2 \ldots T_6$	Scintillation counters	10.1	×	10.1	×	0.5
$M_1 \ldots M_7$	Spark modules	10.1	×	10.1	×	0.6
$A_{1,2}$; $A_{3,4}$	Scintillation counters	79	×	79	×	1.0
$\alpha_1 \alpha_2 .. \delta_1 \delta_2$	Scintillation counters	76	×	79	×	1.0
$\bar{S}_3$	Scintillation counter			20.3 diam	×	1.0
	Spark modules (γ ray)	76	×	76	×	1.0
	Pb sheets (converter)			average 0.94 g/cm^2		
S_c	Scintillation counter in H_2 target			10 diam	×	10.0
S_L	Scintillation counter in H_2 target			7.6 diam	×	0.012

TABLE II

Measurement of Beta Decay Branching Ratio

Source	Efficiency	Events - Background	Background	$R \times 10^8$	Experimental Emphasis
LRL[2]	0.0086 ± ?	10	1 ± ?	2.0 ± 0.6	Angular correlation of gamma rays and annihilation quanta from positron
CERN[10]	(1) 0.040 ± 0.0045	38	6 ± 2	1.15 ± 0.22[(a)]	Energy of gamma rays and positron spectrum
	(2) 0.032 ± 0.005	14	2 ± 1.3		
Columbia[13]	0.047 ± 0.005	36	3 ± 1	0.97 ± 0.20	Angular correlation of gamma rays
CERN[11]	0.18 ± 0.007	165	37 ± 5	1.17 ± 0.12	Energy of gamma rays and positron spectrum
Dubna[12]	0.105 ± 0.014	43	9 ± ?	1.1 ± 0.2	Energy of gamma rays and positron spectrum
LRL-SLAC	0.037 ± 0.003	38	8 ± 3	1.07 ± 0.21	Angular correlation of gamma rays

(a) $R \times 10^8$ for CERN measurement (2) above: 1.7 ± 0.5

FIGURE CAPTIONS

1. Schematic of experimental apparatus showing arrangement of counters S_1, S_2, $\bar{C}$, T, $\bar{S}_3$, stopping spark chambers M, energy degrader D, and γ-ray detectors consisting of lead sheet converters, spark chambers and counters $\alpha, \beta, \gamma, \delta$.

2. Illustration of method of production and transport of pion beam. Vertical focussing is produced by fringe field of bending magnets and horizontal focussing by ends of quadrupole triplet.

3. Response of a γ-ray scintillation counter as voltage is varied. Counter was in coincidence with similar counter on opposite side of pion stopper and was responding to converted γ-rays produced by stopping π^- in indicated substances.

4. Response of π^o detection system to radiation produced by stopping π^- in C and CH_2; γ-ray signals are delayed through gate following π^- stop. (Width of gate was enlarged when taking beta decay data.)

5. Measured number of events with opening angle ($\theta_{2\gamma}$) between the γ-rays originating in $\pi^- + p \rightarrow \pi^o + n$ events. Histogram is best fit to data obtained by folding the experimental resolution into the theoretical distribution and varying $\theta_{2\gamma max}$ and σ_g.

6. Scatter plot and projections of events which have a decay pulse in stopping counters. About 90% of data belonging in Zones I, II and IV has been displayed.

7. Scatter plot and projections of all events except those having a decay pulse satisfying $|t_d - t_\gamma| > 5$ nsec. About 90% of data is displayed in Zone I.

8. Drawing of hydrogen pressure vessel. π^- were stopped between S_L and S_c, generating π^o that were used to calibrate the γ-ray detectors.

9a. Number of π^- stopping in H_2 versus H_2 pressure.

9b. Number of pictures and number of acceptable events due to $\pi^- + p \rightarrow \pi^o + n$ as the H_2 pressure is varied.

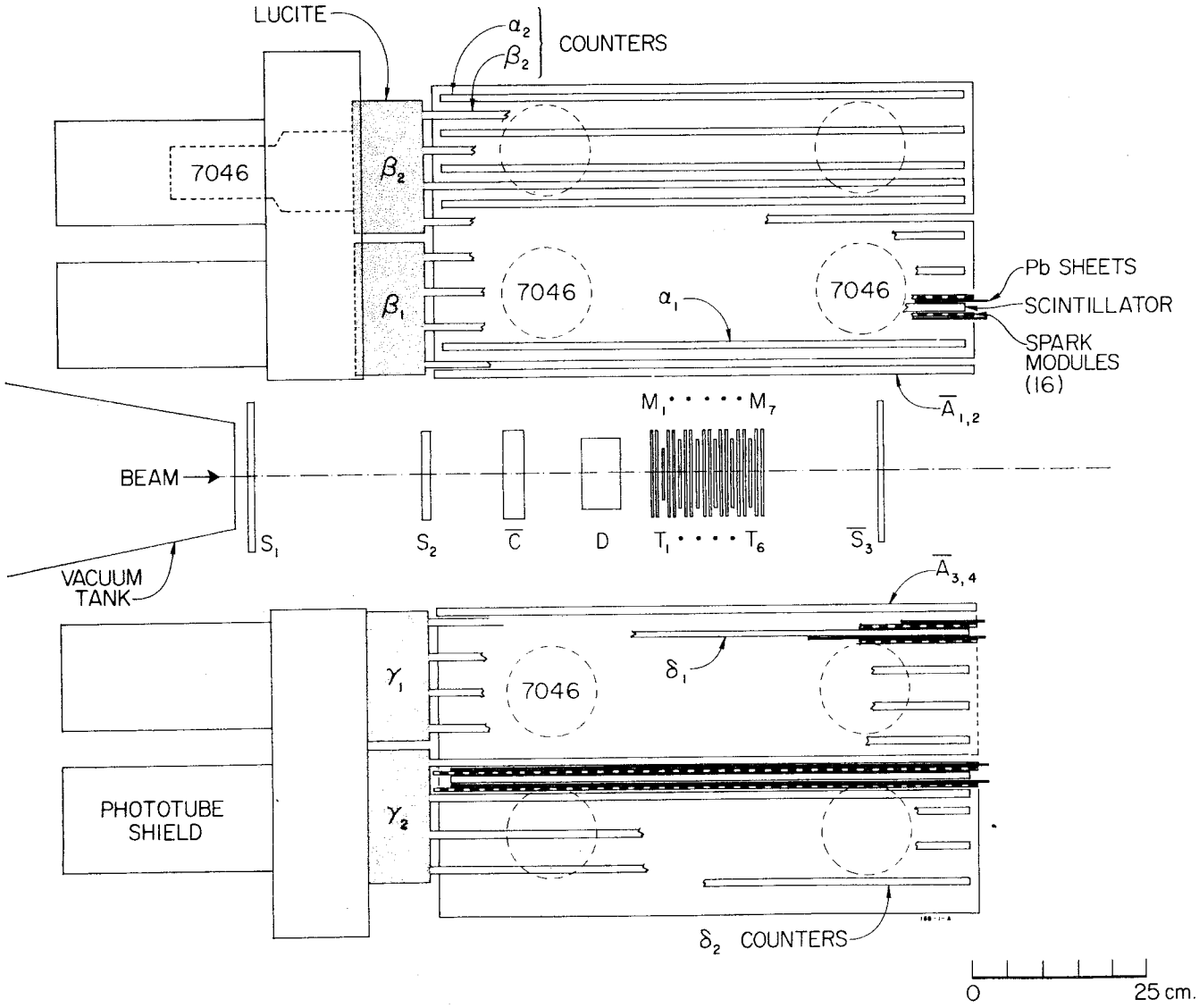
LUCITE
α_2
β_2
COUNTERS
7046
β_2
β_1
7046
α_1
7046
Pb SHEETS
SCINTILLATOR
SPARK MODULES (16)
$M_1 \cdots M_7$
$\overline{A}_{1,2}$
BEAM
S_1
S_2
$\overline{C}$
D
$T_1 \cdots T_6$
$\overline{S}_3$
VACUUM TANK
$\overline{A}_{3,4}$
γ_1
7046
δ_1
PHOTOTUBE SHIELD
γ_2
δ_2 COUNTERS
0
25 cm.

FIG. 1

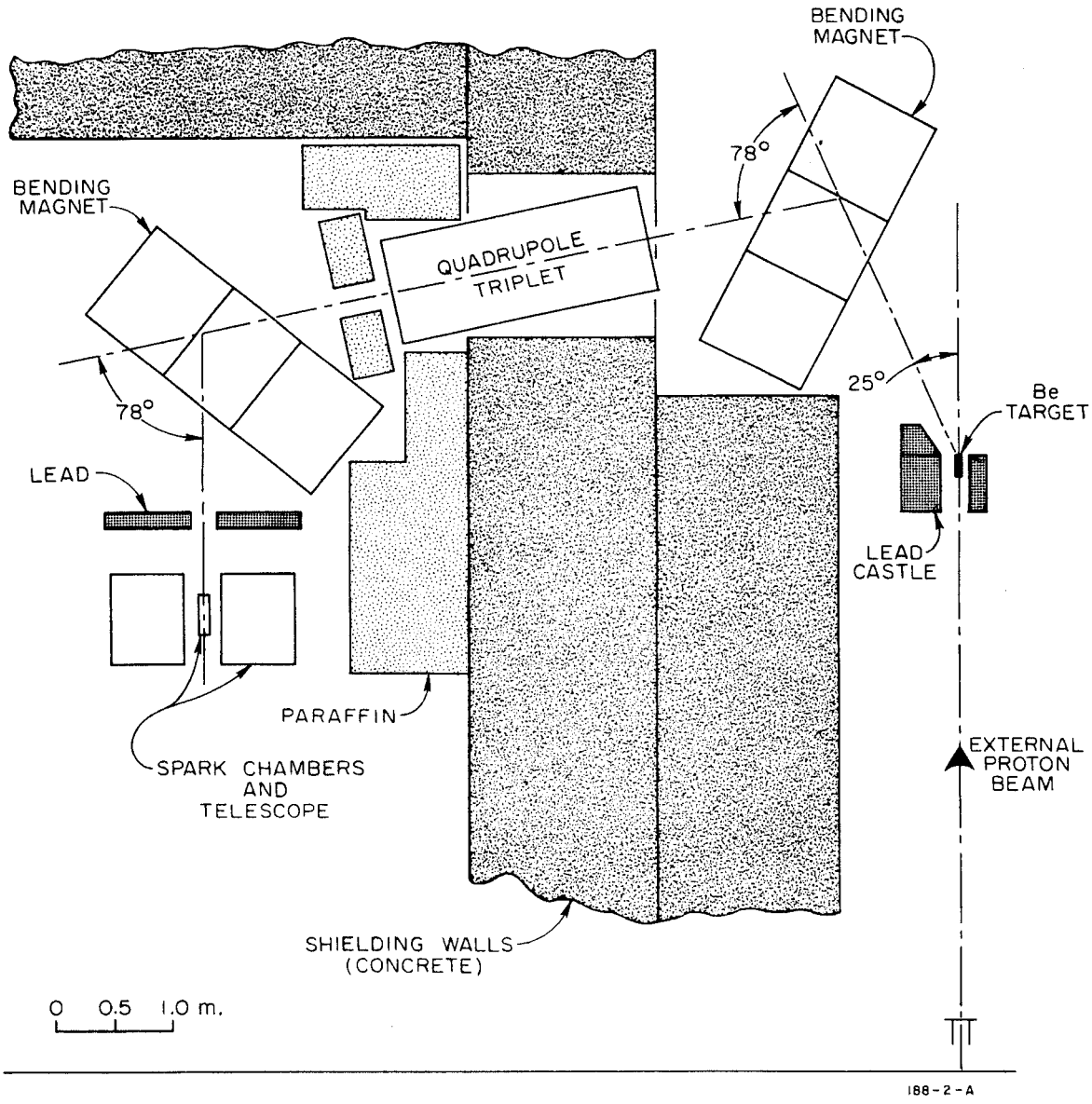

FIG. 2 - BEAM LAYOUT

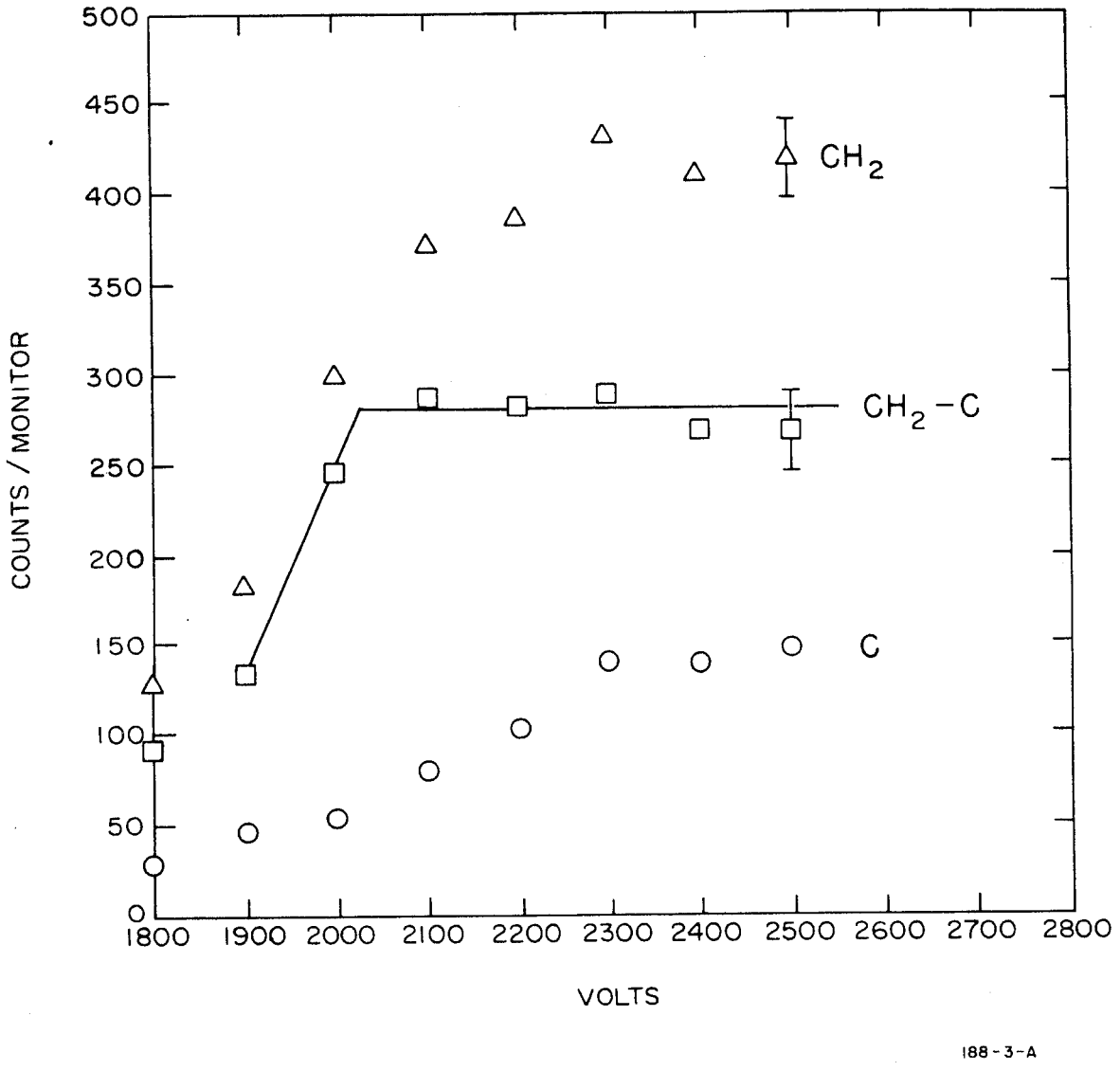
500
450
400
350
300
250
200
150
100
50
0
COUNTS / MONITOR
1800
1900
2000
2100
2200
2300
2400
2500
2600
2700
2800
VOLTS
CH2
CH2 - C
C
188-3-A

FIG. 3

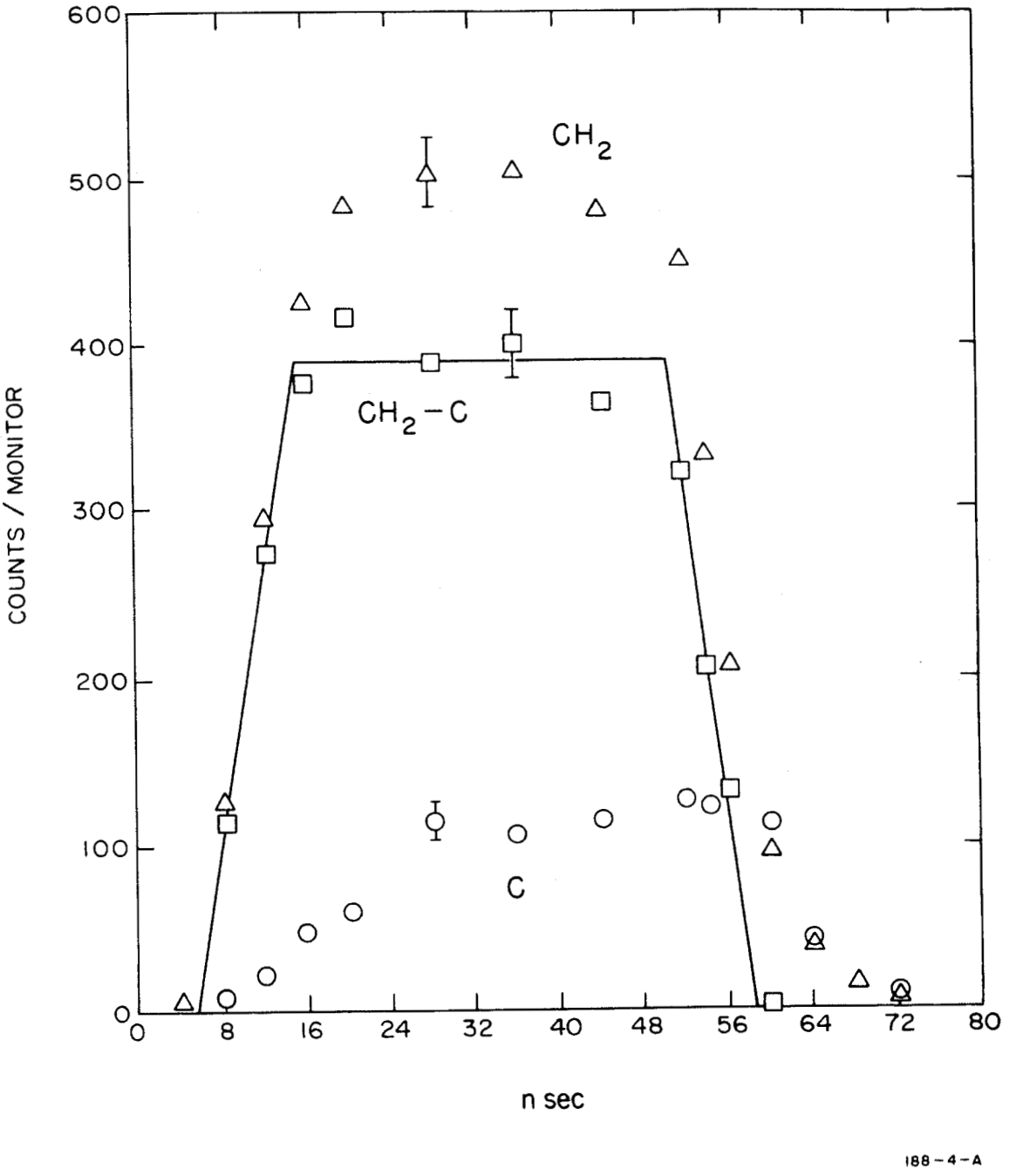
600
500
400
300
200
100
0
COUNTS / MONITOR
CH_2
CH_2-C
C
0
8
16
24
32
40
48
56
64
72
80
n sec
188-4-A

FIG. 4

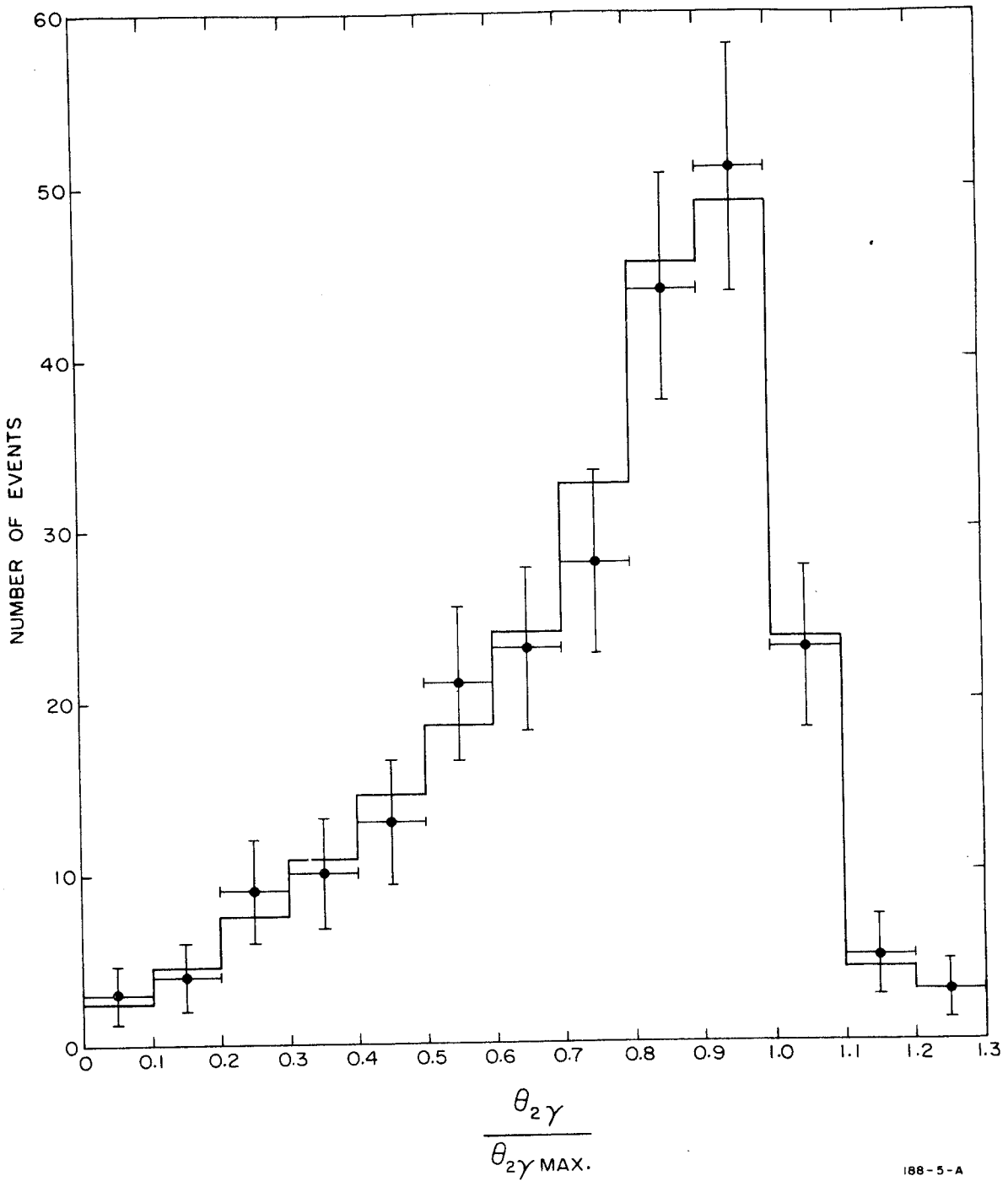
60
50
40
30
20
10
0
NUMBER OF EVENTS
0
0.1
0.2
0.3
0.4
0.5
0.6
0.7
0.8
0.9
1.0
1.1
1.2
1.3
$\frac{\theta_{2\gamma}}{\theta_{2\gamma\,MAX.}}$
188-5-A

FIG. 5

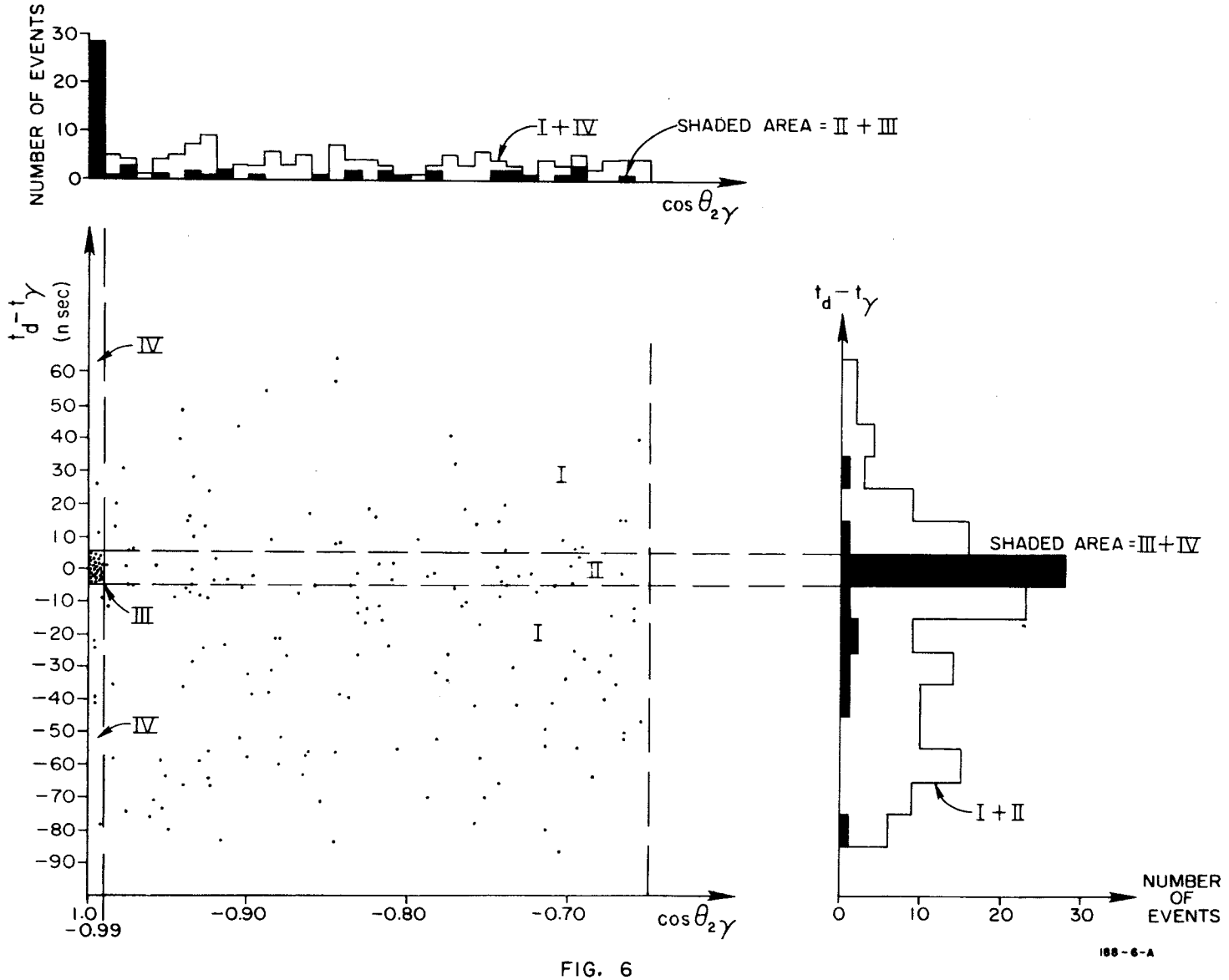
NUMBER OF EVENTS
30
20
10
0
I + IV
SHADED AREA = II + III
cos θ2γ
td − tγ (n sec)
IV
60
50
40
30
20
10
0
−10
−20
−30
−40
−50
−60
−70
−80
−90
I
II
III
IV
I
1.0
−0.99
−0.90
−0.80
−0.70
cos θ2γ
td − tγ
SHADED AREA = III + IV
I + II
0
10
20
30
NUMBER OF EVENTS
168-6-A

FIG. 6

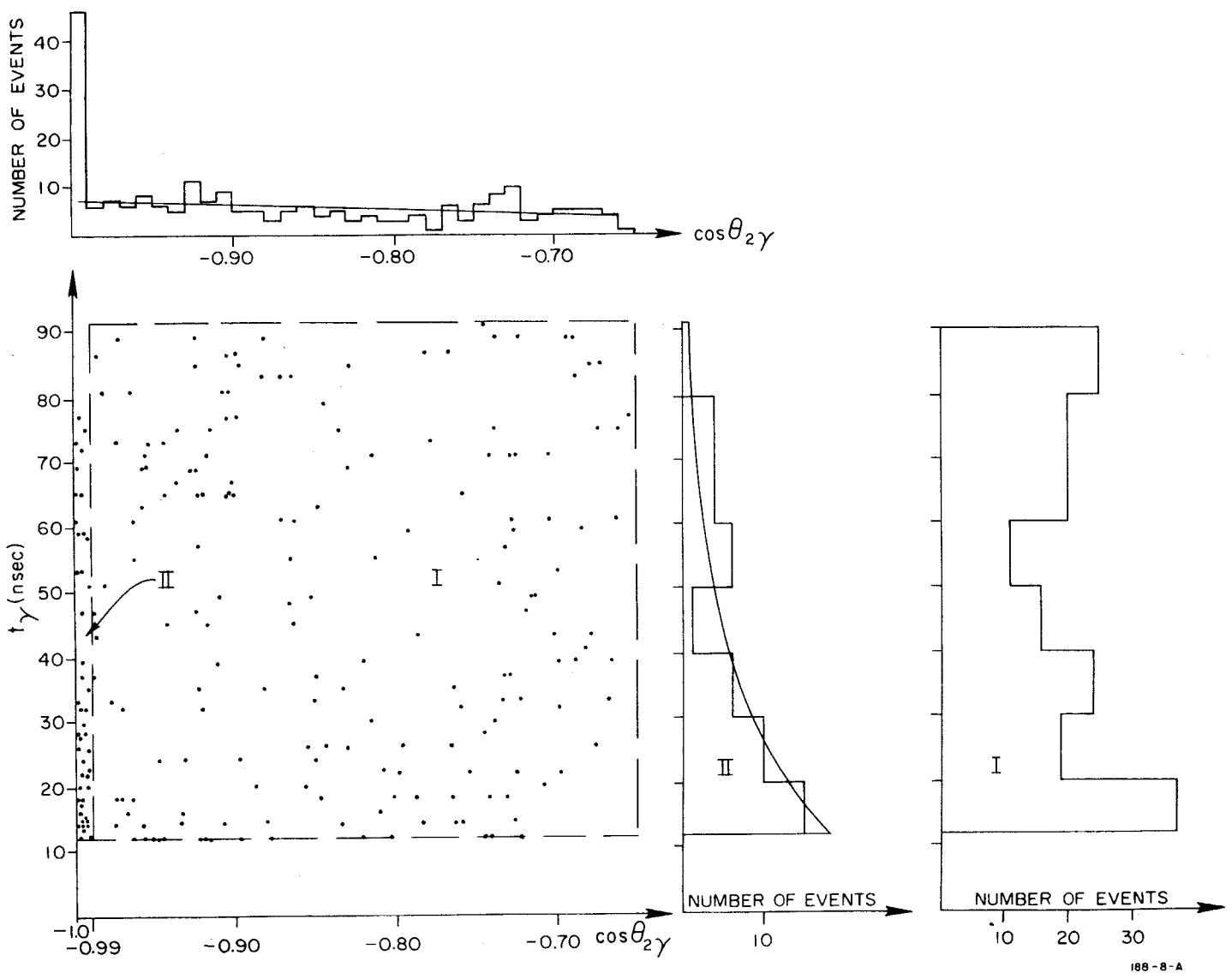
NUMBER OF EVENTS
40
30
20
10
-0.90
-0.80
-0.70
cos θ 2γ
90
80
70
60
50
40
30
20
10
t γ (nsec)
II
I
-1.0
-0.99
-0.90
-0.80
-0.70
cos θ 2γ
NUMBER OF EVENTS
10
II
NUMBER OF EVENTS
10
20
30
I
188-8-A

Fig. 7

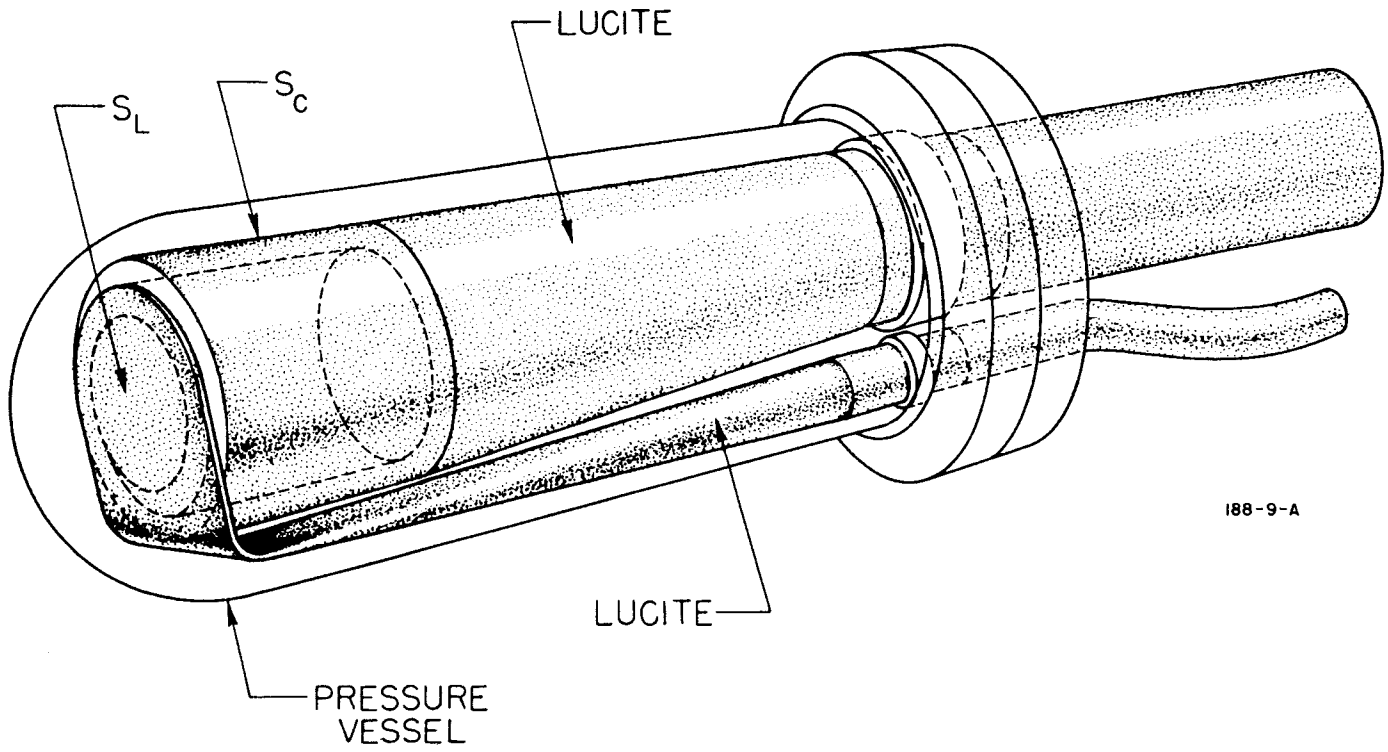

Fig. 8

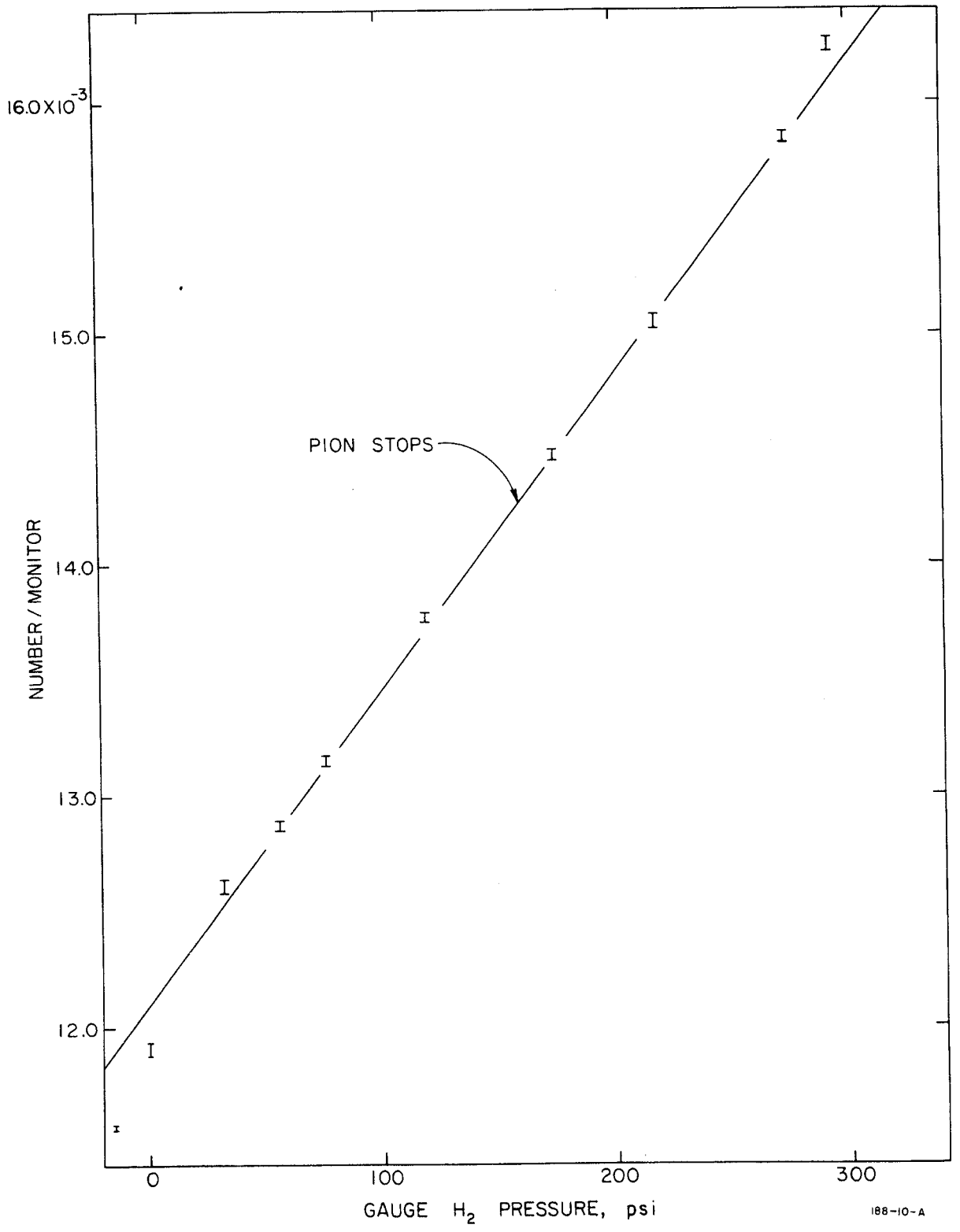
16.0X10^-3
15.0
14.0
13.0
12.0
NUMBER / MONITOR
PION STOPS
0
100
200
300
GAUGE H2 PRESSURE, psi
188-10-A

Fig. 9a

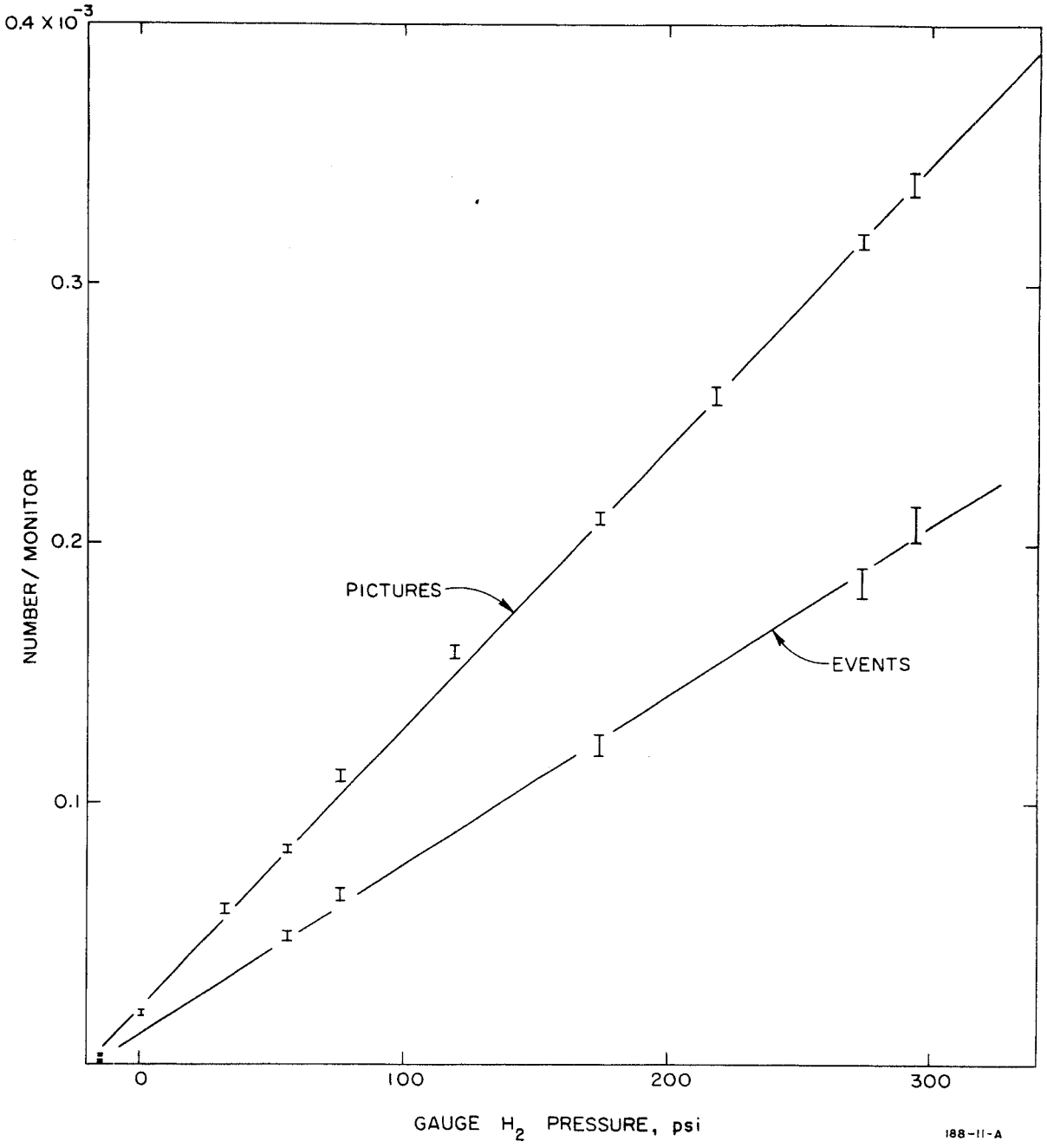
0.4 X 10⁻³
0.3
0.2
0.1
NUMBER / MONITOR
PICTURES
EVENTS
0
100
200
300
GAUGE H2 PRESSURE, psi
188-11-A

Fig. 9b